

# Polarization-controlled contrasted images using dye-doped nematic liquid crystals

R. Porras-Aguilar,<sup>1</sup> J.C. Ramirez-San-Juan,<sup>1</sup> O. Baldovino-Pantaleón,<sup>1</sup> D. May-Arrijoja,<sup>1</sup>  
M. L. Arroyo Carrasco,<sup>2</sup> M.D. Iturbe Castillo,<sup>1,2</sup> D. Sánchez-de-la-Llave,<sup>1</sup> R. Ramos-García<sup>1</sup>

<sup>1</sup>Departamento de Optica, Instituto Nacional de Astrofísica, Óptica y Electrónica, Apartado Postal 51 y 216 72000 Puebla, Pue. Mexico

<sup>2</sup>Benemérita Universidad Autónoma de Puebla, Av. San Claudio y Río Verde 72570 Puebla, Puebla, Mexico  
[rgarcia@inaoep.mx](mailto:rgarcia@inaoep.mx)

**Abstract:** We explore the polarization dependence of the nonlinear response of a planar nematic liquid crystal cell doped with 1% wt of methyl red dye. The results obtained show that the refractive index change can be switched from a positive value to a negative one as the polarization of the beam changes from parallel to perpendicular with respect to the rubbing direction. This property is exploited in a phase contrast system, where a dynamic phase filter is photoinduced in a liquid crystal cell placed in the system's Fourier plane. Real-time contrast inversion in the resulting images is demonstrated.

©2009 Optical Society of America

**OCIS codes:** (160.3710) Liquid crystals; (230.3720) Liquid-crystal devices; (100.5090) Phase-only filters.

---

## References and links

1. Zernike, F., "Diffraction theory of knife-edge test and its improved form, the phase contrast," *Mon. Not. R. Astron. Soc.* **94**, 371-378 (1934).
2. J. Liu, J. Xu, G. Zhang, and S. Liu, "Phase contrast using photorefractive LiNbO<sub>3</sub>:Fe crystals," *Appl. Opt.* **34**, 4972-4975 (1995)
3. J. Joseph, F. J. Aranda, D. V. G. L. N. Rao, J. A. Akkara, and M. Nakashima, "Optical Fourier processing using photoinduced dichroism in a bacteriorhodopsin film," *Opt. Lett.* **21**, 1499-1501 (1996).
4. J. Glückstad, "Phase contrast image synthesis," *Opt. Commun.* **130**, 225-230 (1996).
5. M. D. Iturbe Castillo, D. Sánchez-de-la-Llave, R. Ramos García, L. Olivios-Pérez, L. A. González, M. Rodríguez-Ortiz "Real-time self-induced nonlinear optical Zernike-type filter in a bacteriorhodopsin film," *Opt. Eng.* **40**, 2367-2368 (2003).
6. K. Sendhil, C. Vijayan, M. P. Kothiyal. "Spatial phase filtering with a porphyrin derivate as phase filter in an optical image processor" *Opt. Commun.* **251**, 292- 298 (2005).
7. K. Harada, M. Itoh, S. Kotova, A. Naumov, A. Parfenov, T. Yatagai. "Nonlinear image self-filtering with liquid crystal spatial light modulator" *Opt. Las. Tech.* **30**, 147-155 (1998).
8. K. Komorowska, A. Miniewicz, J. Parka F. Kajzar "Self-induced nonlinear Zernike filter realized with optically addressed liquid crystal spatial light modulator" *J. Appl. Phys.* **92**, 5635-5641 (2002).
9. M. Y. Shih, A. Shishido and I. C. Khoo, All-optical image processing by means of photosensitive nonlinear liquid crystal film: edge enhancement and image addition/substraction, *Opt. Letts.* **26**, 1140-1142 (2001).
10. I.C. Khoo, J. Ding, A. Diaz, Y. Zhang, "Recent studies of optical limiting, image processing and near-infrared nonlinear optics with nematic liquid crystals," *Mol. Cryst. Liq. Cryst.* **375**, 33-44 (2002).
11. C. S. Yelleswarapu, S. R. Kothapally, F. J. Aranda, D.V.G.L.N. Rao, Y. R. Vaillancourt, B. R. Kimball. "Phase contrast imaging using photothermally induced phase transitions in liquid crystals" *Appl. Phys. Lett.* **89**, 211116 (2006).
12. C. G. Treviño-Palacios, M. D. Iturbe-Castillo, D. Sánchez-de-la-Llave, R. Ramos-García, L. I. Olivios-Pérez, "Nonlinear common-path interferometer: an image processor," *Appl. Opt.* **42**, 5091-5095 (2003)
13. I. Janossy, A. L. Lloyd, B. S. Wherret, "Anomalous optical Freedericksz transition on an absorbing liquid crystal," *Mol. Cryst. Liq. Cryst.* **179**, 1-12 (1990).
14. I.C. Khoo, S. Slussarenko, B. D. Guenther, M. Y. Shih, P. H. Chen, W. V. Wood, "Optically Induced Space Charge Fields, DC Voltage, and Extraordinarily Large Nonlinearity in Dye-doped Nematic Liquid Crystals," *Opt. Lett.* **23**, 253-255 (1998).

15. L. Luchetti, M. Di Fabrizio, O. Francescangeli, F. Simoni, "Colossal optical nonlinearity in dye doped liquid crystals," *Opt. Commun.* **233**, 417-424 (2004).
  16. R. Ramos-Garcia, I. Lazo-Martínez, I. Guizar-Iturbide, A. Sanchez-Castillo, *M. Buffety*, P. Rück, "Colossal Nonlinear Optical Effect in Dye-Doped Liquid Crystals," *Mol. Cryst. Liq. Cryst.* **454**, 179-185 (2006).
  17. M. Sheik-Bahae, A.A. Said, T.H. Wei, D.J. Hagan, and E.W. Van Stryland, "Sensitive measurement of optical nonlinearities using a single beam," *IEEE J. Quantum Electron.* **26**, 760-769 (1990).
  18. A.A. Rodriguez Rosales, R. Ortega Martinez, M. L. Arroyo Carrasco, E. Reynoso Lara, C. G. Treviño-Palacios, O. Baldovino-Pantaleon, R. Ramos Garcia, M. D. Iturbe Castillo, "Neither Kerr nor thermal nonlinear response of dye doped liquid crystal characterized by the Z-scan technique". *Mol. Cryst. Liq. Cryst.*, Vol **489**, 9-21 (2008).
  19. E. Reynoso Lara, Z. Navarrete Meza, M. D. Iturbe Castillo, C. G. Treviño Palacios E. Marti Panameño and M. L. Arroyo Carrasco "Influence of the photoinduced focal length of a thin nonlinear material in the Z-scan technique". *Opt. Express* **15**, 2517-2529 (2007).
  20. I. Jánossy and L. Szabados "Optical reorientation of nematic liquid crystals in the presence of photoisomerization" *Phys. Rev. E* **58**, 4598-4604 (1998).
- 

## 1. Introduction

Imaging and visualization of phase objects is of considerable interest in several research fields but it is particularly relevant in microscopy where visualization of transparent specimens is critical to the study of cell and subcellular components and processes. Interferometric techniques are commonly used to extract phase information; however they are cumbersome to work with due to the careful alignment of the system. Zernike phase contrast technique converts phase modulation caused by an object into amplitude modulation by phase shifting the Fourier spectra of the phase object [1]. The Zernike phase contrast system is an imaging system in which a delta-like filter is placed at the center of its Fourier plane. Ideally, the filter induces a phase delay between the spectral component corresponding to the zero spatial frequency and the rest of the spectrum. The consequence of this filtering process is the superposition of a plane wave, generally denominated as synthetic reference wave, and the phase object field distribution at the system image plane. Therefore, the detected intensity at the image plane is no longer constant but modulated by the phase distribution. Zernike phase contrast (PC) can be considered as a common path interferometer since the signal and synthetic reference beam travels along the same optical path. Thus, PC combines the high sensitivity of interferometric techniques and the robustness of common path interferometers which make it insensitive to vibrations.

The use of phase filters based on nonlinear Kerr materials has proven to be highly successful for PC applications. Nonlinear PC blends the robustness of the phase contrast methods, with an optical nonlinear intensity-dependent medium, and the usefulness of the traditional interferometric techniques to measure and visualize phase objects. Phase filters for image processing have been implemented in a variety of materials including photorefractive crystals [2], bacteriorhodopsin films [3-5], dyed liquids [6], electronically and optically addressed spatial light modulators, [7,8] and liquid crystals [9-11]. The obvious advantages of nonlinear phase filters over the standard ones are its easy implementation, self-aligned nature, and tunability. However, if the phase structure that creates the filter possesses relatively low energy at the center of its Fourier spectrum, an adequate filter may not be achieved. One way to alleviate this problem is to illuminate the object beyond its support (fill factor <1), which creates a relatively high energy at the center of the Fourier plane [12].

Among the many materials where phase contrast has been demonstrated, dye doped nematic liquid crystals (DDNLC) are probably the best candidate due to its colossal nonlinearity [13-16] which make it attractive for extremely low power operation (few  $\mu\text{W}$ 's) and relative fast response time (msec). Additional control parameters like temperature, electric field and dopants make them attractive for various optoelectronics information display and processing devices.

In this paper, we characterize the nonlinear response of a dye doped liquid crystal cell made of 5CB doped with methyl red in a planar configuration and implemented it as a phase filter for phase contrast applications. The nonlinear characterization was performed with the Z-scan technique using a cw He-Ne laser at 633 nm. The results demonstrated that the magnitude of the photoinduced phase delay can be controlled not only by the beam's power but also by the light's polarization. In addition, the sign of the nonlinearity can be switched from negative to positive as the light polarization is changed from parallel (to the rubbing direction) to perpendicular. This fact, is particular relevant for phase contrast applications since the contrast of the images can be controlled at will. Implementing this nonlinear filter on a standard microscope, allows all-optical real-time imaging of dynamic events.

## 2. Nonlinear optical characterization of the sample

The liquid crystal employed in our experiments is the nematic 4-pentyl-4'-cyanobiphenyl (5CB, Merck) liquid crystal. The 5CB was doped with methyl red (MR, Aldrich) at a concentration of 1.0% per weight. Glass substrates were cleaned thoroughly. A thin film of poly-vinyl alcohol was spin-coated and then unidirectionally rubbed using a piece of velvet. Thin film spacers of 20  $\mu\text{m}$  were used. Finally, the cell was filled up by capillarity.

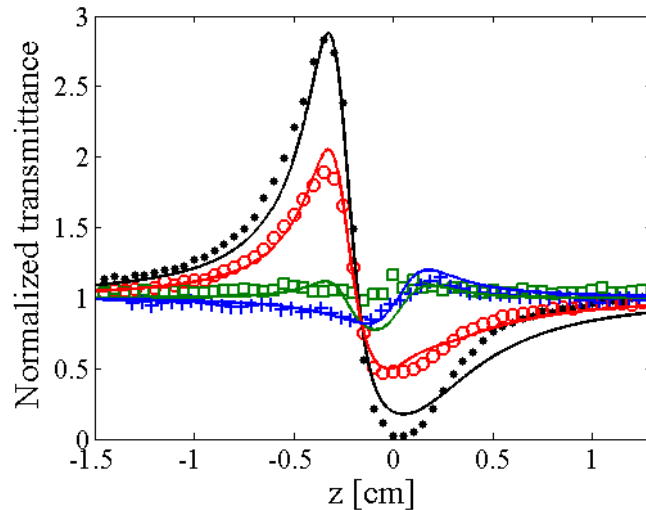


Fig. 1. Z-scan curves at 633 nm for incident polarizations of:  $0^\circ$  ( $\bullet$ ),  $30^\circ$  ( $\circ$ ),  $60^\circ$  ( $\square$ ) and  $90^\circ$  ( $\+$ ). A 3.5 cm lens and unexpanded beam (0.8 mm diameter) from a He-Ne laser ( $\lambda=633$  nm) were used. Sample thickness 20  $\mu\text{m}$  and incident power of 4 mW. Lines are numerical simulations for the same input polarizations. See text for details.

The nonlinear response of the samples was measured using the z-scan technique [17]. As it was demonstrated in a previous paper [18], the nonlinear response of this type of samples is neither Kerr nor thermal in origin. However, its nonlinear optical response is described approximately by a saturated Kerr-like nonlinearity (as will be shown below) and therefore a suitable material for nonlinear phase contrast applications. Experimental results for an incident power of 4 mW and different input polarizations are shown in Fig.1.  $0^\circ$  polarization means that the incident polarization and the rubbing direction are parallel and  $90^\circ$  means polarization perpendicular to the rubbing direction. The amplitude and shape of the Z-scan curve strongly depends on the input polarization. The asymmetry on the Z-scan curves for  $0^\circ$  polarization indicates a large value of the nonlinear phase. This is quite remarkable since the wavelength of the laser ( $\lambda=633$  nm) lies outside the absorption band of the MR. Nevertheless the absorption coefficient is small, is large enough to produce significant photoisomerization

of the dye and causes an optical torque on the liquid crystal host. The sign of the nonlinearity is switched from negative to positive nonlinearity as the input polarization changes from  $0^\circ$  to  $90^\circ$ . The turning point occurs for a polarization of  $\sim 70^\circ$ , where the nonlinearity is negligible. The normalized peak-to-valley transmittance ( $\Delta T_{p-v}$ ) for  $0^\circ$  polarization is almost an order of magnitude larger than that for orthogonal polarization. Since the sign of the nonlinearity can be controlled with the light's polarization, the contrast of the images can, in principle, be controlled at will.

By using a theoretical model described in Ref.19, valid for small and large phase modulation, where the sample can be considered as a thin lens with a photoinduced focal length dependent on the Gaussian beam radius  $\omega^m$  (where  $m=3$ ) it is possible to calculate the on-axis phase change  $\Delta\Phi_0$  from the Z-scan curve as  $\Delta T_{p-v}=3\Delta\Phi_0$ . Fig.2, shows the obtained photoinduced phase against the input power for an input polarization of  $0^\circ$  and  $90^\circ$ . In both cases the magnitude of the on axis phase change increased with the input power. The negative phase seems to saturate earlier than the positive one but it was not possible to determine its saturation power due to the limited output power of our laser.

Our polarization-dependent Z-scan results can be readily understood considering the model developed by Janossy [20] to explain the directional dependence of the enhancement factor of the optical torque in azo dye-doped nematic liquid crystal. In this model, the *trans* and *cis* isomers contribute independently to the optical torque as opposed to antroquinone dyes.

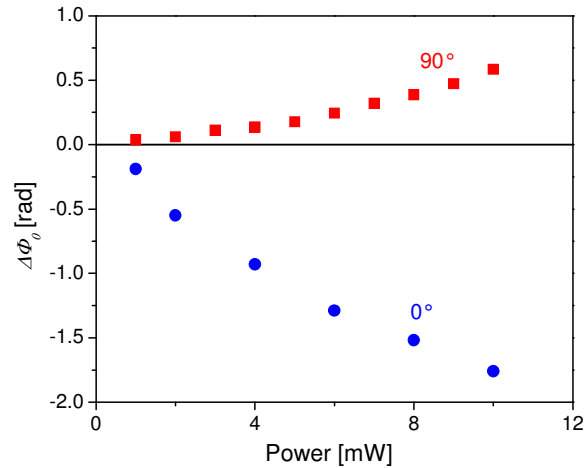


Fig. 2 Photoinduced phase change for  $0^\circ$  (●) and  $90^\circ$  (■) polarization as function of the incident power

The relative population of *trans* and *cis* populations depend on the angle between the polarization direction of the light wave and the director, which is assumed to be parallel to the rubbing direction. Thus, the enhancement factor in this model is described by

$$\eta = X\eta_c + (1 - X)\eta_T \quad (1)$$

where X is fraction of the *cis* isomers and  $\eta_c$  and  $\eta_T$  are the enhancement factors for the *cis* and *trans* isomers, respectively. These factors have no angular dependence and for the liquid crystal E63 doped with 0.3% of the dye R4 take the values  $\eta_c = 650$  and  $\eta_T = -410$  [20]. The fraction of *cis* isomers possess an angular dependence given by [20]

$$X = X_{ord} \frac{1 + g \cos^2 \Psi}{1 + h \cos^2 \Psi} \quad (2)$$

where  $X_{ord}$  is the *cis* fraction generated by an ordinary polarized beam,  $\Psi$  is the angle between the polarization vector and the director vector, and  $g$  and  $h$  are molecular parameters determined from transmission measurements. This model can be used to explain the Z-scan experiments by considering that the effective photoinduced on-axis phase change follows a similar expression to Eq. (1). The dependence of the effective on-axis phase change with the input polarization can be assumed as

$$\Delta\Phi = X\Delta\Phi_N + (1 - X)\Delta\Phi_P \quad (3)$$

where  $\Delta\Phi_N$  and  $\Delta\Phi_P$  are the on axis phase changes for  $0^\circ$  and  $90^\circ$  input polarizations, respectively. Considering this dependence, the values of the constants that better reproduce the experimental data, are given by:  $g=9$ ,  $h=0.1$ ,  $X_{ord}=0.1$ , with these values it is possible to demonstrate that the effective on axis phase change can be approximated to

$$\Delta\Phi \approx \cos^2 \Psi \Delta\Phi_N + \sin^2 \Psi \Delta\Phi_P \quad (4)$$

The results of the simulation are shown in Fig.1 and describe quite well the experimental data. Under these conditions, numerical simulations were realized in order to evaluate the contrast obtained for a binary phase object. The object was a square with a  $0.5\pi$  rad phase change with respect to the surrounding area phase. In order to ensure optimal contrast, the fill factor i.e. the object area divided by the total illuminated area was 0.1 [5]. The filter phase distribution was obtained by Fourier transforming the phase object and calculating its intensity distribution. Since saturation effects were not considered, the filter phase distribution was identical to the phase object Fourier transform intensity distribution. In the Fourier plane, a saturable Kerr media was used and the maximum filter phase for each incident polarization angle was obtained from Eq. (4) using the data shown in Fig. 2. Finally, the inverse Fourier transform of the filtered phase distribution is taken to obtain the intensity distribution on the output plane. The image contrast was calculated as  $(I_i - I_o)/(I_i + I_o)$ , where  $I_i$  is the intensity inside the square and  $I_o$  the intensity outside the square. By using this expression, contrast inversion is observed whenever a change in the contrast sign appears. The results obtained are shown in Fig. 5. As it can be observed, for the three intensities analyzed, contrast inversion is obtained for an incident polarization angle larger than  $70^\circ$ .

### 3. Phase contrast experiments

The experimental set-up used to visualize microscopic objects is shown in Fig. 3. The beam from a linearly polarized He-Ne laser ( $\lambda=633\text{nm}$ ) was employed as the illuminating source. In order to control the polarization and power of the beam, a variable neutral density filter and a half wave plate, respectively, were employed. The body of a microscope with a 20X objective and a 10X ocular was employed to produce a 200X magnification imaging system. The liquid crystal cell was placed at the Fourier plane of the input image which occurs just after the eyepiece. A CCD camera was used to capture the contrasted images.

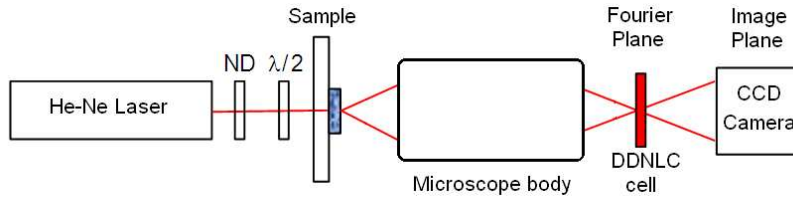


Fig. 3. Experimental set-up for the phase contrast microscope. DDLNC is the dye doped liquid crystal cell.

In order to determine the operational range of our phase contrast microscope, several phase objects were etched on glass plates ( $n=1.5$ ). The objects were squares pools of  $100 \times 100 \mu\text{m}^2$  and different depths ( $\lambda$ ,  $\lambda/2$ ,  $\lambda/4$ ,  $\lambda/8$ ,  $\lambda/20$  and  $\lambda/40$ , where  $\lambda=0.633 \text{ nm}$ ). As an example, Fig. 4 shows the phase contrasted images for the  $\lambda/2$  depth square which has a phase difference of  $0.5\pi$  rad. The contrast was measured from the images following the expression  $C=(A_i - A_o)/(A_i + A_o)$  where  $A_i$  and  $A_o$  represent the average intensity values inside and outside the square, respectively. The number on the figures indicates the angle between the rubbing direction and polarization vector. For  $0^\circ$  polarization (negative nonlinearity) the phase object looks bright with a dark background. For  $70^\circ$  the contrast practically disappears and only the borders of the object are clearly visible, while for  $90^\circ$  (positive nonlinearity) the contrast of the image is reversed.

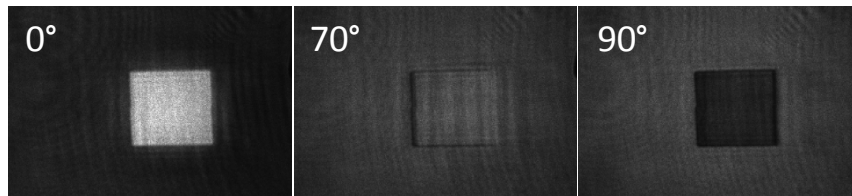


Fig. 4. Contrast image of  $100 \times 100 \mu\text{m}^2$  objects etched on glass with a depth of  $320 \text{ nm}$  ( $\sim \lambda/2$ ). The numbers on the top left corner corresponds to the angle between the rubbing direction and the polarization vector of the laser beam. For negative nonlinearity the object is bright on a dark background, for an intermediate angle of  $70^\circ$  the contrast almost disappears while for positive nonlinearity the contrast is reversed. (Media 1)

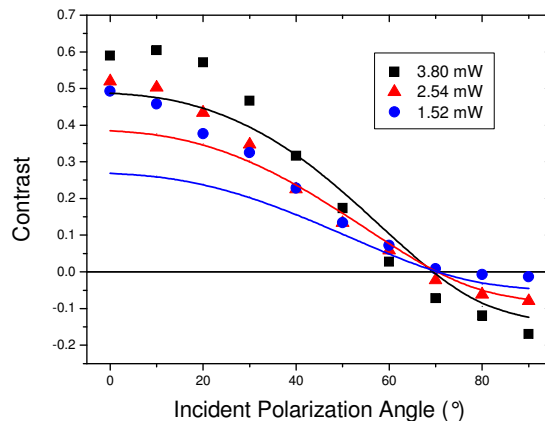


Fig. 5. Contrast as function of the polarization of the incident beam for different input powers of: 3.8 (■), 2.54 (▲) and 1.52 (●) mW for a phase object of  $\lambda/2$  thickness. Continuous lines represent the contrast obtained from our model for the same power level.

The minimum object depth that can be contrasted is  $\lambda/8$ . However, the contrast is limited by the light scattering produced by the liquid crystal cell sample rather than by our detection system. The scattering is produced by the rubbed polymer so better sample preparation is likely to increase the detectable object's depth.

Contrast inversion was observed for all incident powers, as it is shown in Fig. 5. It can be observed that, due to the competition between the positive and negative nonlinearity, for an angle of almost  $70^\circ$  the contrast obtained was very small which is consistent with the Z-scan measurements. The continuous lines correspond to the contrast obtained from our model. The overall behaviour is qualitatively similar to the numerical results presented in the previous section.

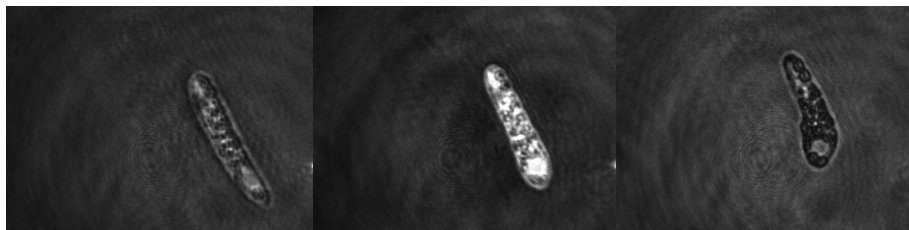


Fig. 6. Real time images of biological specimens (paramecium) obtained by the nonlinear phase microscope. The  $\lambda/2$  plate was rotated in order to improve the contrast. The size of the living organisms is  $\sim 75 \mu\text{m}$ . (Media 2).

The proposed system can be used to visualize phase objects where contrast of the images can be changed in order to enhance different components of the image. Biological samples may contain objects with spatially changing phases, and hence they are good candidates to demonstrate the performance of the system with dynamic events. Fig. 6 (Media 2), shows some biological specimens (*Paramecium*, a unicellular ciliate protozoa) observed in the nonlinear phase contrast microscope. These images have been obtained in real time and rotating the  $\lambda/2$  plate. As we can see, the contrast can be adjusted in real time to observe some specific detail in the phase objects.

#### 4. Conclusions

We described a phase contrast system where the phase filter was implemented using a planar cell of liquid crystal 5CB doped with methyl red. The phase of such filter, for illumination at 633 nm, can be switched from positive to negative by changing the incident polarization with respect to the cell director vector and its magnitude can be controlled with the incident power. Real time operation offered by this technique allows dynamic visualization of living organisms. We have observed an inversion in the contrast for a binary phase object and in microorganisms. The phase contrast can be easily implemented in standard microscopes without further complications.

#### Acknowledgements

This work was supported by CONACyT Grant #45950 and financial funding from Merck Mexico. We thank Prof. Patrick L. LiKamWa and CREOL for the facilities given for the fabrication of the phase objects.